Materials Advances

ROYAL SOCIETY OF CHEMISTRY

PAPER

View Article Online
View Journal

Cite this: DOI: 10.1039/d5ma01500f

Robust and biocompatible radiative cooling textiles based on a synergistic TiO_2 and SiO_2 nanoparticle coating

Rayan Ghazi, [a] Fatimah Samman, [a] Tadd Truscott [b] and Dana Alsulaiman *[a]

Radiative cooling textiles offer a passive strategy for reducing heat load and improving thermal comfort, yet achieving durable coatings with high solar reflectivity and mid-infrared emissivity remains challenging. Here we develop a composite TiO_2–SiO_2 nanoparticle coating for cotton fabrics, using polyacrylic acid-based functionalization strategy to promote uniform, stable nanoparticle adhesion. Nanoparticle sizes were rationally selected based on Mie-scattering calculations, identifying 200 nm TiO_2 for optimal solar scattering and 50 nm SiO_2 for enhanced emissivity. The resulting coated fabrics exhibited significantly higher reflectance across the solar spectrum and strong emission within the 8–13 μm atmospheric window. Outdoor measurements showed temperature reductions of up to 6.9 °C under direct sunlight relative to uncoated cotton, with consistent performance over multiple days. The results are comparable to or exceeding reductions reported in prior nanoparticle-based or photonic textile systems. Cytotoxicity assays of nanoparticle dispersions and fabric extracts confirmed biocompatibility with human dermal fibroblasts, supporting suitability for wearable applications. These findings demonstrate a scalable, durable, and biologically safe radiative-cooling textile with potential for energy-efficient personal thermal management.

Received 22nd December 2025,
Accepted 1st March 2026

DOI: 10.1039/d5ma01500f

rsc.li/materials-advances

1 Introduction

Global warming continues to intensify thermal stress across climates, increasing the demand for sustainable approaches to personal cooling and energy efficient textile technologies. Rising ambient temperatures have led to greater reliance on air conditioning and other active cooling systems, substantially increasing energy consumption and associated greenhouse gas emissions. This has stimulated growing interest in passive thermal management strategies that can reduce personal heat load without external energy input.[1–3] Radiative cooling has emerged as a highly promising strategy because it dissipates heat from a surface directly to outer space through thermal emission in the mid-infrared (MIR) atmospheric window (8–13 μm) while minimizing solar heat gain.[4–6] Exploiting this mechanism in wearable fabrics offers a pathway toward enhanced thermal comfort during outdoor activities without external power input.[5–7]

Various inorganic oxides, including ZnO, MgO, Al_2O_3, and $CaCO_3$, have been investigated for radiative cooling applications.[8–10] ZnO-based textile coatings exhibit high solar reflectance and mid-infrared (mid-IR) emissivity; however, their performance can be compromised by absorption losses that depend on particle structure and synthesis route.[11] MgO coatings and paints are attractive due to their strong phonon–polariton-related infrared emission, making them promising radiative coolers.[12] Nevertheless, achieving flexible and durable textile-compatible coating requires careful optimization of binders and processing conditions.[9] Al_2O_3 has also been incorporated into radiative-cooling composites and films, though its effectiveness is often dependent on composite architecture and thickness, which can complicate its integration into thin, soft textile substrates without affecting fabric hand-feel.[10] $CaCO_3$ (chalk) has recently gained attention for passive personal cooling on cotton *via* scalable coatings; however, it typically relies on microstructural design and high particle loading to achieve broadband solar scattering, and its long-term adhesion and wash durability remain formulation dependent.[13]

In this work, TiO_2 and SiO_2 were selected due to their complementary optical roles, which are particularly advantageous for wearable radiative-cooling textiles.[14] Specifically, (i) TiO_2 provides strong solar backscattering when its particle size is tuned to the solar spectrum, enabling high reflectance with

[a] *Materials Science and Engineering Program, Physical Science and Engineering Division, King Abdullah University of Science and Technology (KAUST), Thuwal 23955-6900, Saudi Arabia. E-mail: rayan.ghazi@kaust.edu.sa, dana.alsulaiman@kaust.edu.sa*

[b] *Mechanical Engineering, Physical Science and Engineering Division, King Abdullah University of Science and Technology (KAUST), Thuwal 23955-6900, Saudi Arabia. E-mail: tadd.truscott@kaust.edu.sa*

minimal absorption losses, and (ii) SiO_2 offers strong mid-IR emission through vibrational (phonon-related) resonances within the atmospheric transparency window (8–13 μm), while remaining largely transparent in the visible range when used at subwavelength dimensions.[15,16] This design strategy aligns with established nanoparticle-based radiative-cooling systems, in which TiO_2 primarily governs solar reflectivity and SiO_2 contributes to thermal emission in the sky window. More broadly, effective daytime radiative cooling requires the simultaneous suppression of solar absorption and enhancement of thermal emission through the atmospheric window.

Recent progress in nanotechnology-enabled textiles has demonstrated that metal oxide nanoparticles can simultaneously increase solar reflectivity and enhance long-wavelength thermal emissivity.[7,17,18] TiO_2 nanoparticles efficiently scatter visible and near-infrared sunlight due to their high refractive index, whereas SiO_2 nanoparticles provide strong MIR emissivity.[17,18] Several studies have achieved notable sub-ambient cooling using nanoparticle coatings or photonic structures—for example, temperature reductions of approximately 4.7 °C to 12 °C have been reported for coated fabrics or functional membranes under direct sunlight.[19–22] These results highlight the potential of nanoparticle-based radiative cooling textiles; however, they also reveal key limitations. Many reported systems rely on complex multilayer designs, require specialized fabrication methods, or lack durability when applied to flexible substrates.[23] Moreover, optimization of nanoparticle size is rarely grounded in theoretical scattering analysis despite its strong influence on optical performance.[4,24–28]

A further challenge concerns wearability and human safety. Radiative cooling fabrics place nanoparticles in direct contact with skin, yet the cytotoxicity of nanoparticle-coated textiles remains insufficiently characterized. Existing reports show that some metal oxides exhibit size- and concentration-dependent cytotoxic responses in dermal cells, underscoring the need for standardized biocompatibility assessment.[29–32] To date, only a small number of studies have evaluated cytotoxicity in the context of textile coatings, and even fewer have examined nanoparticle leaching through extract-based assays that reflect realistic exposure pathways.[30,31]

Addressing these gaps, the present study develops a hybrid TiO_2–SiO_2 nanoparticle coating for cotton fabrics that simultaneously enhances solar reflectivity and MIR emissivity while maintaining flexibility and durability. Nanoparticle sizes were rationally selected using Mie-scattering calculations, providing a theoretical foundation for maximizing solar scattering efficiency. A polyacrylic acid-based functionalization strategy was employed to enable robust adhesion of the hybrid nanoparticles to the cotton fibers, improving coating stability and durability. The resulting fabrics were evaluated *via* thorough materials characterization, morphological characterization, outdoor radiative cooling measurements, and *in vitro* cytotoxicity assessments using human dermal fibroblasts (HDFs) to ensure suitability for wearable applications. This integrated approach advances the design of nanoparticle-based radiative cooling textiles by combining theoretical optimization, experimentally validated cooling performance, and systematic biocompatibility testing.

2 Materials & methods

2.1 Cytotoxicity assessment

2.1.1 Cell culture. Human dermal fibroblast (HDF) cells were cultured in low glucose DMEM (GlutaMAX™, pyruvate) supplemented with 10% fetal bovine serum (FBS) and 1% penicillin/streptomycin. Cells were maintained at 37 °C in 5% CO_2. Media were changed every 48 h, and cells were subcultured upon reaching $>80\%$ confluency.

2.1.2 Preparation of nanoparticle dispersions. Commercially available TiO_2 and SiO_2 nanoparticle powders were used in this study without further synthesis. TiO_2 nanoparticles (rutile phase, $\geq 99.5\%$ purity, average particle size of 200 nm) were purchased from Nanografi Nano Technology (Turkey), while SiO_2 nanoparticles with an average particle size of 50 nm were obtained from Shilpent (India). According to the suppliers' specifications, both nanoparticle powders exhibit narrow particle size distributions consistent with the reported average sizes. Prior to use, TiO_2 and SiO_2 nanoparticle powders were UV-disinfected for 1 h. Stock dispersions were prepared at a concentration of 2 mg mL^{-1} in supplemented DMEM, with 1% (v/v) DMSO added to ensure homogeneous nanoparticle dispersion. The dispersions were sonicated for 15 min and gently inverted before each dilution to maintain uniform distribution. Nanoparticles were subsequently diluted in supplemented DMEM as detailed in Table S1 (SI) and immediately added to cells for the cell counting kit-8 (CCK-8) assay.

2.1.3 Preparation of extracts. For material disinfection and coating preparation, bare cotton was immersed in several changes of 70% ethanol, boiled in deionized water, then processed for different non-functionalized and functionalized coatings as detailed Table S2 (SI). Extracts were prepared according to ISO 10993-12, using an extraction ratio of 3 cm2 of cotton fabric per 1 mL of media. Cotton fabric was UV-disinfected for 1 h on each side prior to extract preparation. Following ISO 10993-5, cotton pieces were immersed in non-supplemented DMEM and incubated at 37 °C for 1 and 3 days with mechanical agitation at 250 rpm (Thermal Mixer, Thermo Scientific). Negative (non-supplemented DMEM) and positive (40% v/v DMSO in non-supplemented DMEM) controls were prepared similarly. Extracts were centrifuged at 7300 rpm (Centrifuge 5225 R, Eppendorf) for 10 min at room temperature to remove any loose fabric or large particles that could damage cells or interfere with CCK-8 results Fig. S2, SI).

2.1.4 CCK-8 viability assay. The CCK-8 assay was performed following the manufacturer's protocol (Abcam). Details for nanoparticle dispersions and extracts are provided in Table S3 (SI). Briefly, HDF cells were seeded at a density of 8000 cells per well in a 96-well plate and incubated overnight at 37 °C in 5% CO_2. Treatments, including different concentrations of nanoparticle dispersions, extracts, and the respective controls,

were added in triplicates and incubated at 37 °C in a 5% CO_2 environment for 24 h. After treatment, media were removed, and cells were washed twice with 100 μL PBS (with Ca^{2+} and Mg^{2+}). Supplemented DMEM containing CCK-8 reagent (10 μL per 100 μL of media) was added to each well (100 μL), including wells without cells for background correction. Plates were incubated for 4 h at 37 °C in 5% CO_2, then 80 μL of the mixture were transferred to a new 96-well plate to avoid interference from nanoparticle aggregates or debris. The absorbance ratio at 570 nm and 605 nm was measured using a microplate reader (Varioskan Lux, Thermo Scientific). Blank well absorbance was subtracted to correct for background. Cell viability was calculated relative to the untreated control wells (100% viability) using the formula:

$$\text{Cell viability } (\%) = \frac{A_{\text{treated}}}{A_{\text{control}}} \times 100 \quad (1)$$

2.1.5 Live/dead assay and morphological studies. Nanoparticle treatments at different concentrations were added in triplicates alongside an untreated control, followed by incubation at 37 °C in 5% CO_2 for 48 h. Cells were then processed for live/dead assay and morphological analysis at room temperature. For live/dead assay, media were replaced with staining solution containing 18 μM fluorescein diacetate (FDA) and 1 μM ethidium homodimer-1 (EthD-1) in supplemented DMEM, and cells were incubated for 15 min. Staining solution was replaced with supplemented DMEM for imaging using brightfield (BF) and fluorescent channels (FITC: ex. 495 nm/em. 519 nm; Texas Red: ex. 592 nm/em. 614 nm) on an inverted microscope (Axio Observer, Zeiss).

Morphological assessment was performed by an Alexa Flour™ 488-phalloidin following the manufacturer protocol (Invitrogen). Cells were washed twice with PBS, fixed with 100 μL of 4% methanol-free formaldehyde solution containing 3 μm DAPI in PBS for 15 min, then washed twice with PBS. Permeabilization was performed using 0.1% Triton™ X-100 in PBS for 15 min, followed by two PBS washes. Cells were then incubated with Alexa Flour™ 488-phalloidin (1× in PBS) for 30 min, washed twice with PBS, then imaged using BF and fluorescent channels (Alexa Fluor 488: ex. 493 nm/em. 517 nm; DAPI: ex. 353 nm/em. 465 nm) on an inverted microscope (Axio Observer, Zeiss).

2.2 Experimental section

2.2.1 Radiative cooling studies setup. Continuous radiative cooling performance of uncoated and TiO_2–SiO_2 nanoparticle-coated cotton fabrics was evaluated for 5 h on a clear sunny day in February 2025 at the KAUST campus, Thuwal (22.2833°N, 39.1000°E), using a custom-designed outdoor measurement setup (Fig. 1b and c). Each fabric sample was placed on a silicone rubber-insulated heater (Omega, 39 cm^2) to maintain a stable temperature baseline and mounted inside a hardwood frame (40 cm × 40 cm × 15 cm). The interior surfaces of the frame were lined with aluminum foil to enhance reflectivity and reduce unwanted solar heat absorption.

A clear acrylic box (20 cm × 20 cm × 3 cm) was placed above the samples to allow airflow and sunlight while providing environmental shielding. Thermocouples positioned beneath both coated and uncoated fabrics recorded temperature continuously. The combination of foam insulation, acrylic chamber, and rubber sheet minimized external heat exchange, ensuring that temperature differences reflected genuine radiative cooling behavior. Coated and uncoated samples were measured simultaneously under identical conditions using separate enclosures.

2.2.2 Fabric coating procedure. Cotton fabric (100% cotton, plain-woven, 150 GSM) was purchased from SWATCHON and cut into 15 × 15 cm^2 samples. The fabrics received deionized water soaking for 24 hours to eliminate surface contaminants which made them more water-absorbent. The surface modification process used a grafting solution containing acrylic acid (98% extra pure stabilized Thermo Scientific) as the monomer and benzophenone (99% Alfa Aesar) as the photo-initiator which were dissolved in ethanol. The fabric samples were immersed in the solution and bath-sonicated in a beaker under standard laboratory lighting conditions, without intentional UV exposure. This step was separate from the subsequent UV grafting process. The samples were then exposed to UV light at 365 nm (80 W, 10 cm distance) for 5 minutes. The treatment process generated surface radicals, enabling the attachment of carboxyl (–COOH) functional groups to cotton fibers, thereby forming hydrogen bonds for nanoparticle attachment. The preparation involved creating a nanoparticle dispersion containing TiO_2 nanoparticles with an average size of 200 nm and SiO_2 nanoparticles with an average size of 50 nm, at equal weight proportions of 0.5 wt% each relative to the total dispersion volume. The solution mixed for 20 minutes in bath sonication to achieve complete nanoparticle distribution throughout the solution. The functionalized cotton fabrics were then immersed in the nanoparticle dispersion at a fixed liquor-to-fabric ratio and bath-sonicated to promote uniform nanoparticle deposition on the fiber surfaces. The coating process was performed in a single deposition cycle, followed by air-drying at room temperature. The coated fabrics underwent a final step of 99% ethanol rinsing to detach nanoparticles that were not strongly attached, followed by drying at 70 °C for 2 hours before additional testing and characterization.

3 Result & discussion

3.1 Theoretical modeling for optimization of nanoparticle size

Radiative cooling performance depends strongly on the ability of a surface to scatter incoming solar radiation while efficiently emitting in the mid-infrared (MIR) atmospheric window. To rationally select nanoparticle sizes that enhance these effects, Mie-scattering calculations were performed following classical scattering theory.[24–28] These calculations evaluate the wavelength-dependent scattering efficiency Q_{sca} of spherical particles and are commonly used to optimize optical reflectors for radiative cooling.

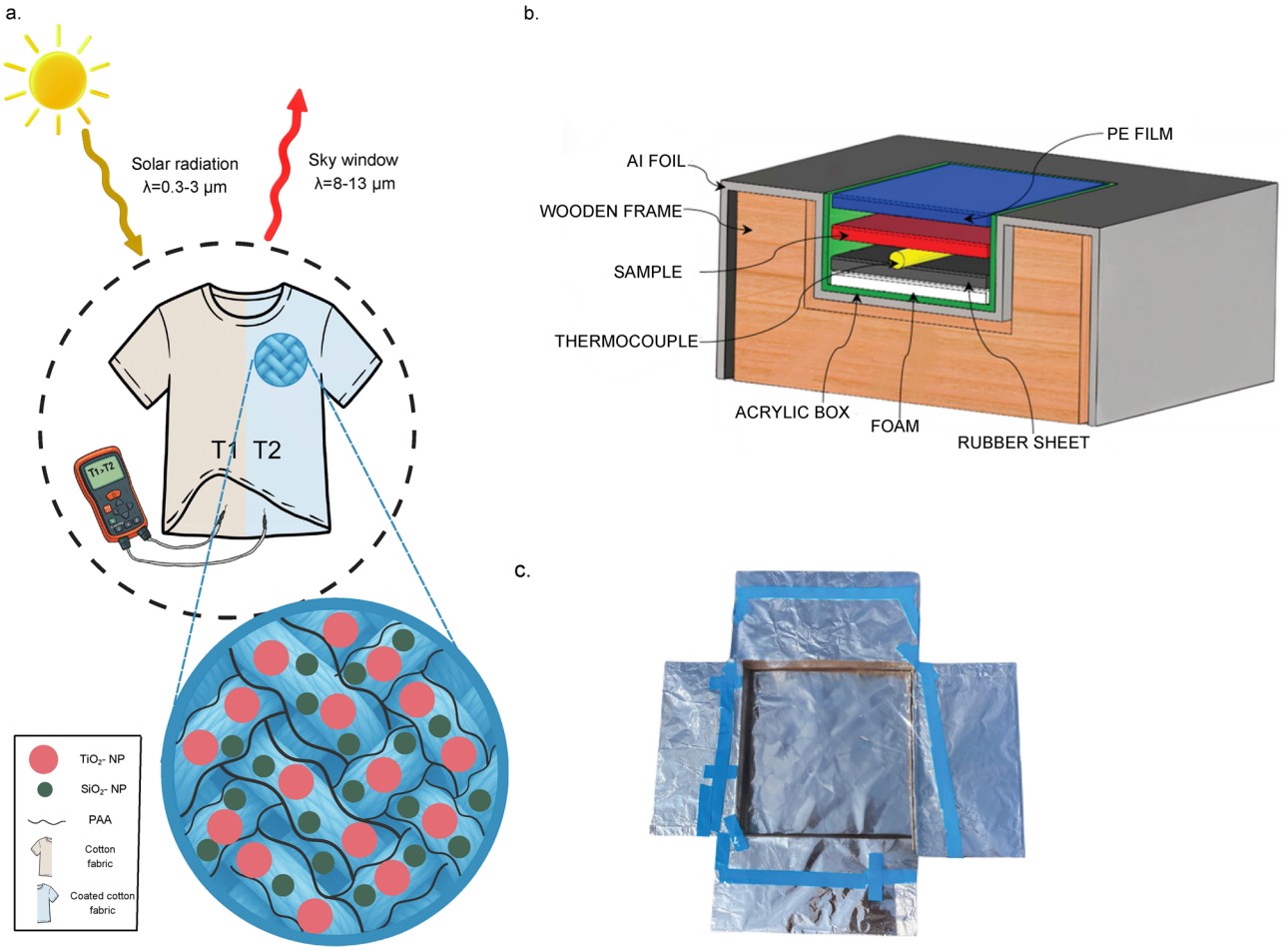

Fig. 1 (a) Schematic illustration of the radiative cooling mechanism in TiO_2–SiO_2 nanoparticle-coated cotton fabrics (PAA = polyacrylic acid; NP = nanoparticle). (b) Schematic illustration and (c) photograph of the experimental setup used to evaluate the radiative cooling performance of uncoated and TiO_2–SiO_2-coated cotton fabrics.

Scattering efficiency was computed for TiO_2 particles with diameters from 50 to 600 nm across the 300–800 nm wavelength range, corresponding to the peak solar spectrum. As shown in Fig. 2a, TiO_2 nanoparticles around 200 nm exhibit strong resonant scattering in the visible regime (300–550 nm), making them highly effective solar backscatterers. This guided the selection of 200 nm TiO_2 as the primary reflective component in the coating.

SiO_2 nanoparticles were incorporated to enhance long-wavelength emissivity. A diameter of 50 nm was chosen based on previous studies demonstrating favorable MIR emissive properties for sub-100 nm SiO_2.[33] Because these particles are significantly smaller than MIR wavelengths, they do not disrupt cotton's intrinsic emissivity in the 8–13 μm atmospheric window. UV-Vis-NIR spectra (Fig. 2b) of the bare (blue) and coated (red) cotton samples confirm the expected optical behavior: the hybrid TiO_2–SiO_2 nanoparticle coating substantially increases reflectance across the 0.3–2.5 μm wavelength window compared to bare cotton. Together, the Mie-guided nanoparticle sizes and complementary optical properties of TiO_2 and SiO_2 nanoparticles form the basis for the enhanced radiative cooling performance observed experimentally.

It should be noted that the Mie-based analysis provides a simplified, guiding description of the optical behavior and does not explicitly account for interparticle coupling effects, which are expected to be minimal at the low nanoparticle loadings employed here.[25] Accordingly, the theoretical modeling is intended to inform nanoparticle size selection rather than to serve as a fully coupled optical model of the composite coating. The experimentally measured reflectance and radiative cooling performance are consistent with the trends predicted by this approach, supporting its validity within the studied concentration range.

3.2 Structural and morphological analysis of nanoparticles

Key considerations in choosing suitable nanoparticles for cotton treatment to achieve radiative cooling include optical properties of a high refractive index and low absorption in the visible light range.[34] A high index promotes increased scattering of visible light to enhance the persistence of the optical path length when sunlight is absorbed, whereas low absorption minimizes heating effects from visible light. Additionally, high emissivity in the 8–13 μm atmospheric window is

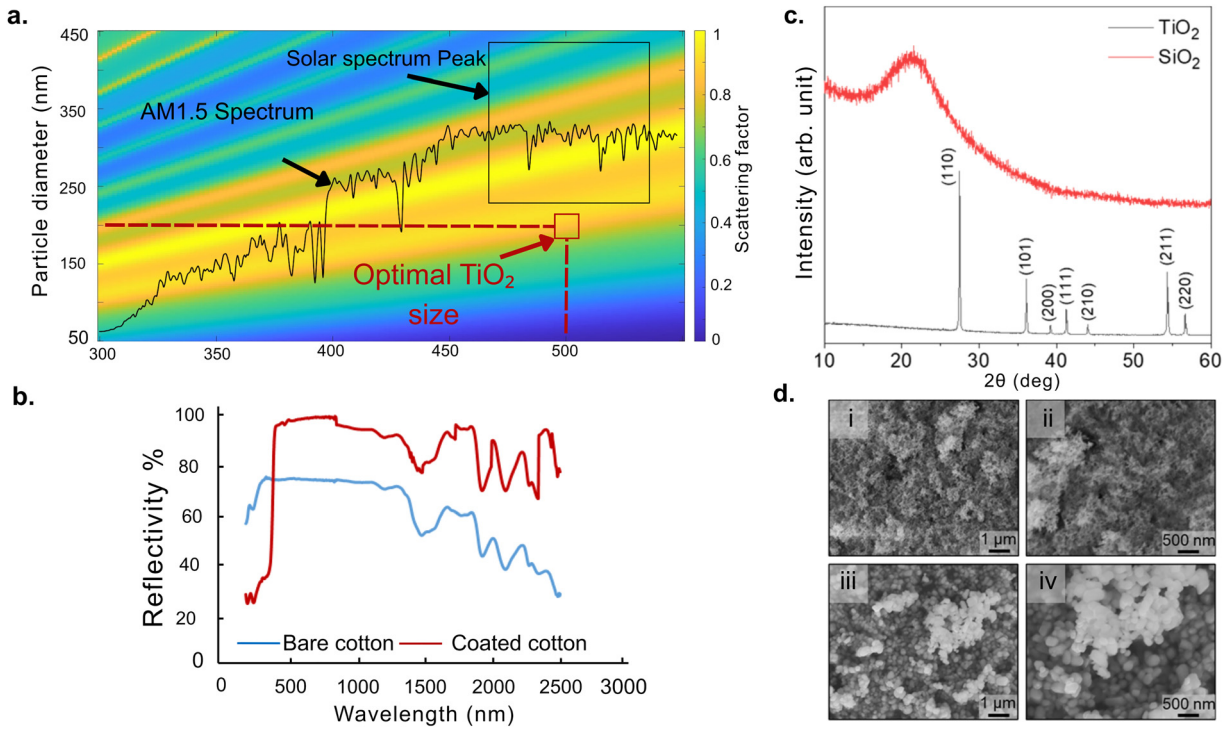

Fig. 2 (a) Theoretical modeling of the scattering efficiency of TiO_2 nanoparticles was performed as a function of particle diameter and wavelength. The resulting heatmap shows that 200 nm TiO_2 nanoparticles exhibit strong scattering in the 300–550 nm wavelength range, which guided the selection of the optimal nanoparticle size for maximizing solar reflectivity. (b) UV-Vis-NIR reflectivity of the bare (blue) and coated (red) cotton samples. (c) XRD patterns of the TiO_2 and SiO_2 nanoparticles. (d) SEM images of (i) and (ii) SiO_2 nanoparticles, and (iii) and (iv) TiO_2 nanoparticles at different magnifications, respectively.

required, where terrestrial transmittance permits radiative heat loss.[35]

The XRD pattern of TiO_2 nanoparticles (Fig. 2c, black profile) exhibits diffraction peaks at 2θ values of 27.4°, 36.1°, 39.2°, 41.2°, 44.1°, 54.3°, and 56.6° corresponding to the (110), (101), (200), (111), (210), (211), and (220) planes, respectively, matching the tetragonal rutile phase (ICDD PDF No. 21-1276; space group: $P4_2/mnm$; a = 4.593 Å, c = 2.959 Å).[36] The sharp, well-defined peaks indicate a higher degree of crystallinity in the nanoparticles, which is crucial for achieving a strong refractive index and, consequently, efficient visible-light scattering. This enhanced scattering reduces solar energy absorption and contributes significantly to the overall radiative cooling performance.[37]

Next, XRD analysis of the SiO_2 nanoparticles revealed only a single broad peak at a 2θ value of approximately 22°, a characteristic peak indicative of their amorphous nature, as shown in Fig. 2c (red profile). Furthermore, no other peaks were observed, confirming the purity of the material. The structural morphology of both nanoparticle samples was analyzed using SEM. Fig. 2d(i) and (ii) show the surface morphology of the SiO_2 nanoparticles at different magnifications. As SiO_2 nanoparticles have a strong agglomeration tendency, the SEM images reveal that the nanoparticles, with an average size of 50 nm, are agglomerated in the powder form. Fig. 2d(iii) and (iv) show the spherical morphology of TiO_2 nanoparticles with minimal aggregation, yielding particle sizes that closely match the optimal geometries based on Mie theory calculations. Together, these structural and optical properties confirm that the TiO_2 and SiO_2 nanoparticles meet the design requirements for hybrid radiative cooling coatings and validate the assumptions used in Section 3.1 for theoretical size optimization.

3.3 Morphological characterization of coated cotton fabrics

SEM images of untreated, non-functionalized, and functionalized coated cotton fabrics (Fig. 3a–c) highlight the influence of surface chemistry on coating uniformity. Bare cotton exhibits smooth fiber surfaces free of contaminants, confirming the effectiveness of our pre-cleaning steps (Fig. 3a). When the TiO_2–SiO_2 nanoparticle dispersion is applied to non-functionalized cotton (Fig. 3b), the coating is non-uniform, with visible nanoparticle clustering and regions of incomplete surface coverage. In contrast, fabrics functionalized with carboxylic acid (–COOH groups) show dense, uniform nanoparticle attachment across entire fibers (Fig. 3c). Polyacrylic acid (PAA) functionalization markedly improves nanoparticle adhesion and reduces particle aggregation, leading to higher coating durability and more consistent optical performance. These results support the use of carboxyl-functionalized substrates for practical radiative cooling textiles.

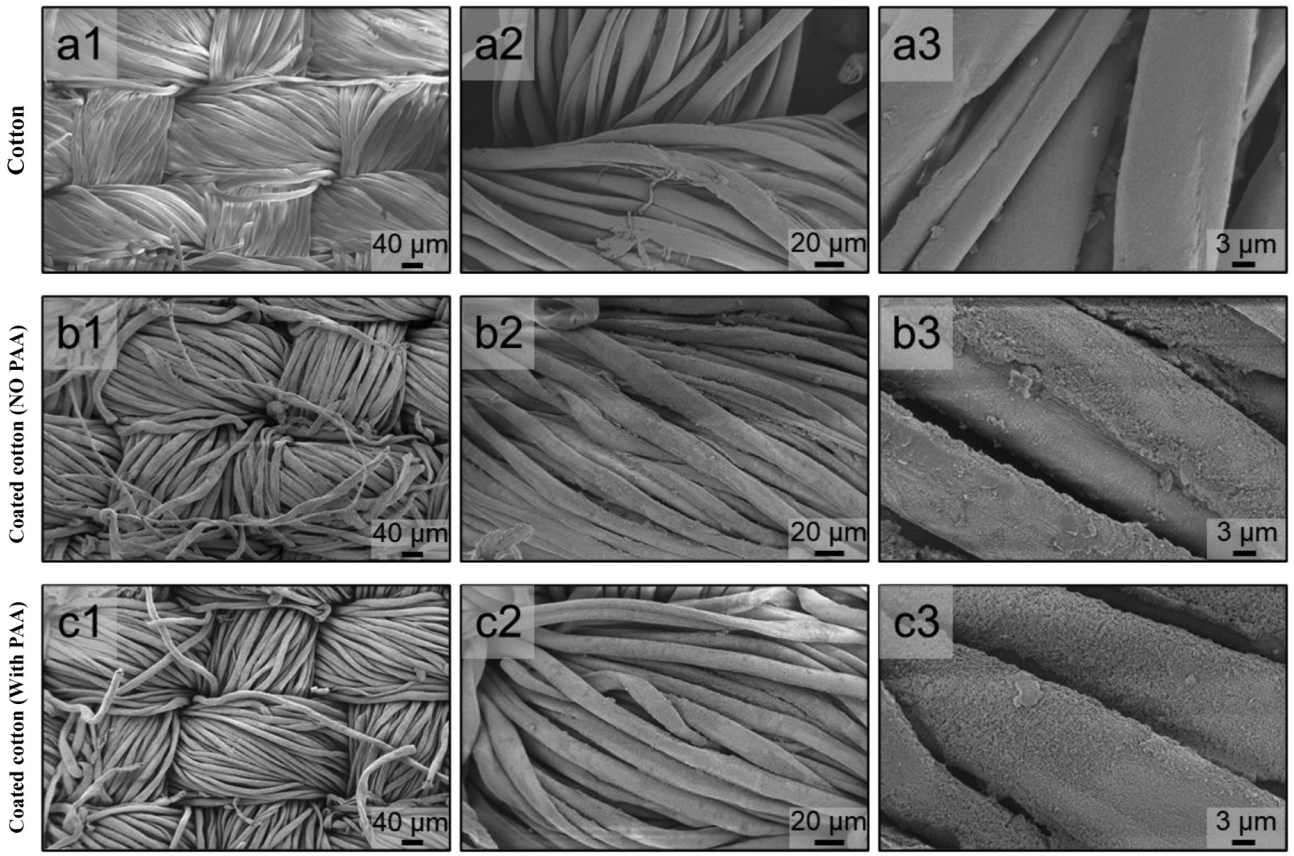

Fig. 3 SEM images showing the surface morphology of bare cotton a(i)–(iii), TiO_2–SiO_2 coatings on non-functionalized fabric b(i)–(iii), and TiO_2–SiO_2 coatings on functionalized fabric c(i)–(iii), respectively, at different magnifications (PAA = polyacrylic acid).

3.4 Chemical composition and durability analysis

Fig. S1 presents the XPS survey spectra of the cotton fabric treated under different conditions. The spectrum (i) of the bare cotton fabric after cleaning (black line), exhibits characteristic peaks of C 1s and O 1s that confirm the organic nature of cellulose, and the absence of surface impurities or residues. Red profile (ii) shows the survey spectrum of a hybrid coating of TiO_2–SiO_2 nanoparticles on the functionalized cotton fabric prior to any washing step. The presence of Ti 2p, Si 2p, along with C 1s and O 1s, confirms the successful deposition of the nanoparticles. When compared to the bare cotton fabric, the coated fabric showed a decrease in the carbon and an increase in the oxygen fraction, indicating that the cellulose-based surface is uniformly covered by the oxide nanoparticle coating. The higher oxygen content also validates the presence of metal oxide nanoparticle coatings on the surface of the fabric.[38]

The calculated Si/Ti atomic ratio (given in Table 1) for the coated fabrics is higher than unity and varies between samples, reaching values of approximately 2–3 in some cases, despite the use of equal weight fractions of TiO_2 and SiO_2 in the coating formulation. This deviation can be attributed to the surface-sensitive nature of XPS analysis ($\sim$5–10 nm probing depth), differences in particle size and surface area, and the distinct dispersion behavior of the nanoparticles. The smaller ($\approx$50 nm), amorphous SiO_2 nanoparticles possess a significantly higher specific surface area compared to the larger ($\approx$200 nm), crystalline TiO_2 particles, which can lead to preferential surface exposure and stronger interfacial interaction with the functionalized cotton fibers. Consequently, SiO_2 is more prominently detected at the outermost surface, resulting in an elevated Si/Ti atomic ratio in the XPS measurements.

Table 1 XPS-derived elemental composition of cotton fabric treated under different conditions

Sample	C (at%)	O (at%)	Si (at%)	Ti (at%)	N (at%)
Bare cotton	59	39	2	—	—
Coated fabric before washing	16	58	18	8	—
Functionalized & coated fabric after washing	24	55	14	7	—
Non-functionalized & coated fabric before washing	20	55	18	7	—
Non-functionalized & coated fabric after washing	34	54	9	3	—

To further validate the durability and stability of our PAA-based functionalization approach, functionalized and non-functionalized fabrics coated with hybrid nanoparticles were analyzed after rigorous washing in ethanol for 1 h. The XPS results for the functionalized fabric after washing, shown in blue profile (iii), indicate that the nanoparticles remained well adhered to the surface of the fabric even after two washing cycles. Notably, the chemical composition of the functionalized and coated fabric remained nearly unchanged before and after washing, demonstrating that the introduction of hydroxyl ions (*via* our PAA functionalization strategy) enabled strong hydrogen bonding interactions with the metal oxide nanoparticles, ensuring robust adhesion to the textile surface. On the other hand, the nanoparticle coating on the non-functionalized fabric showed less stability before washing green profile (iv), where a significant amount of the nanoparticles were removed after washing, as indicated by the decreased content of Si, Ti, and O, and increased content of C atoms (purple profile (v)). This stability is essential for wearable applications, where repeated handling, washing, and environmental exposure can otherwise degrade coating stability and lower cooling performance. The elemental compositions of the cotton fabrics treated under these different conditions are summarized and presented in Table 1.

3.5 *In vitro* cytotoxicity assessment

To evaluate the safety of the hybrid coating for direct skin contact, cytotoxicity was assessed using human dermal fibroblasts (HDFs). Viability after 24 h exposure to pristine nanoparticles remained above the ISO 10993-5 non-cytotoxic threshold of 70% for all tested concentrations except the highest TiO_2 dose (500 μg mL^{-1}), which yielded 66.8% viability (Fig. 4a). These trends are consistent with size- and

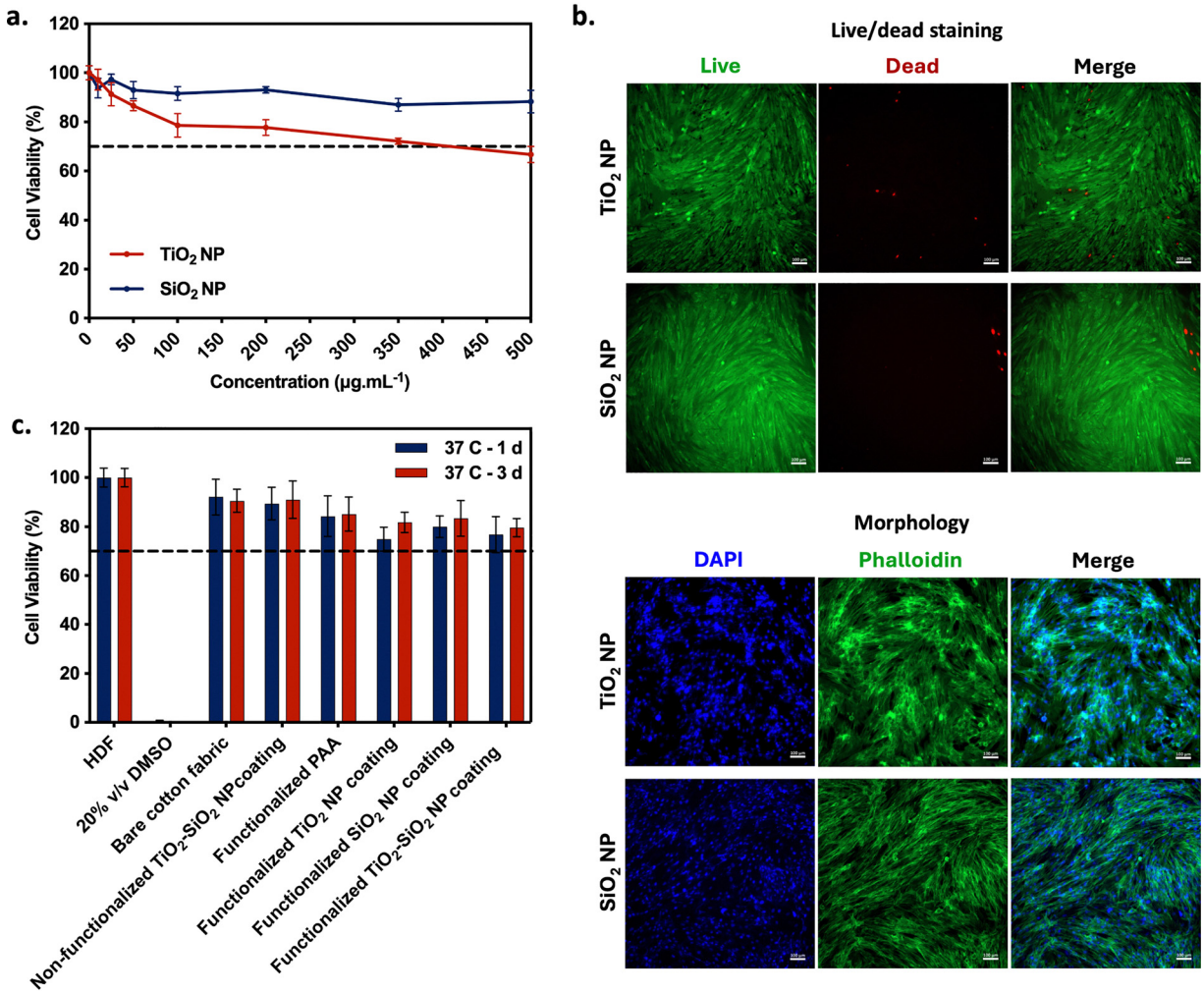

Fig. 4 (a) Cell viability of HDF cells after 24 h of exposure to pristine nanoparticles across a concentration range covering up to 0.5 wt% (500 μg mL^{-1}) used in this study. TiO_2 at 500 μg mL^{-1} resulted in 66.8% viability, slightly below the cytotoxicity threshold (n = 3; error bars: SD). (b) Live/dead and morphology images of HDF cells at 50 μg mL^{-1} (FDA: viable cells; EthD-1: dead cells; DAPI: nuclei; phalloidin: cytoskeleton F-actin filaments), showing predominantly viable cells with normal morphology following 48 h of exposure. Scale bar: 100 μm. (c) Cell viability following 24 h of exposure to cotton-coating extracts (1 and 3 days at 37 °C) (n = 6, mean of six replicates averaged from two independent experiments, each with three replicates; error bars: SD). In all plots, the dashed line indicates the 70% cytotoxicity threshold.

concentration-dependent effects reported for metal oxide nanoparticles.[29–32]

Live/dead fluorescence imaging (Fig. 4b) further confirmed that cells retained healthy morphology, intact cytoskeletons, and predominantly live-cell staining after exposure to nanoparticles.

Extracts of coated fabrics, prepared according to ISO 10993-12, showed no cytotoxic effects for either 1-day or 3-day extract durations (Fig. 4c). All viability values exceeded 70%, and HDFs maintained normal spindle-shaped morphology (Fig. S9 and S10). These results indicate that both the pristine nanoparticles at working concentrations and the final coated fabrics are cytocompatible and suitable for wearable applications.

3.6 Measurement of radiative cooling performance

The radiative cooling performance of coated and uncoated cotton fabrics was evaluated under direct sunlight between 10:00 and 15:00 (Fig. 5a and b). The TiO_2–SiO_2 nanoparticle-coated fabric consistently maintained lower surface temperatures than uncoated cotton throughout all measurement periods. The largest temperature reduction occurred at 12:00, when solar irradiance was highest, yielding a maximum cooling of 6.9 °C relative to uncoated cotton. This cooling effect was reproducible over three consecutive days and remained stable despite fluctuations in ambient conditions, confirming the reliability of the coating under realistic outdoor exposure. Infrared thermal imaging further corroborates this behavior (Fig. 5c). The coated cotton clearly exhibits a lower surface temperature (37.8 °C) compared to bare cotton (44.5 °C) under identical illumination conditions, corresponding to a substantial surface temperature difference visible in the thermal contrast. The uniform and cooler temperature distribution across the coated sample also indicates homogeneous nanoparticle coverage and effective suppression of solar heat absorption. In

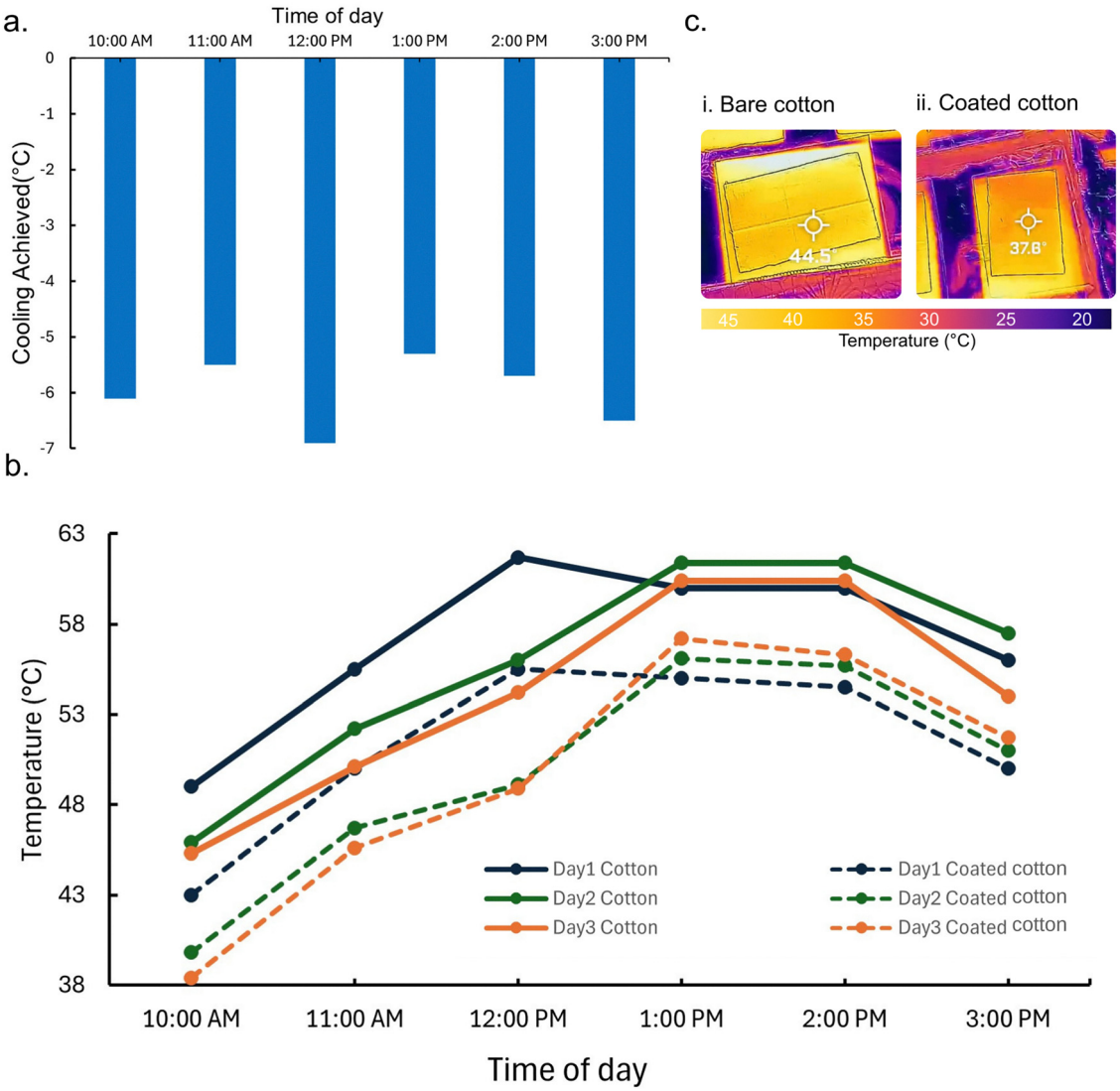

Fig. 5 (a) Comparison of the radiative cooling achieved on a sunny day, which recorded the highest radiative cooling performance, for TiO_2–SiO_2 nanoparticle-coated cotton fabrics (day 2). (b) Comparison of the corresponding radiative cooling performance. (c) Thermal images taken by an IR camera indicating the cooling performance of bare cotton (i) and TiO_2–SiO_2 coated cotton (ii) fabrics.

contrast, the uncoated cotton shows higher localized heat accumulation, consistent with its greater solar absorption and limited radiative heat dissipation. Based on our rational material design, the enhanced cooling performance is attributed to the synergistic action of broadband solar reflectivity from TiO_2 nanoparticles and strong MIR emissivity from SiO_2 nanoparticles, supported by uniform nanoparticle adhesion on the PAA-functionalized cotton fibers. These results demonstrate that the robust TiO_2–SiO_2 hybrid coating effectively reduces thermal load under realistic outdoor conditions and highlight its strong potential for application in personal cooling textiles, particularly in hot climates such as Saudi Arabia and other high-solar-irradiance regions.

Conclusions

This work demonstrates a durable and biocompatible radiative cooling textile enabled by a hybrid TiO_2–SiO_2 nanoparticle coating. Mie-scattering theory guided the rational selection of 200 nm TiO_2 and 50 nm SiO_2 nanoparticles to maximize solar reflectivity and mid-infrared emissivity, respectively, while polyacrylic-acid functionalization of cotton fibers promoted uniform nanoparticle adhesion and enhanced coating stability. The resulting fabrics exhibited high broadband reflectance and strong emissive behavior, achieving up to a 6.9 °C surface temperature reduction compared to bare cotton.

Conflicts of interest

There are no conflicts to declare.

Data availability

The data supporting this article are included in the supplementary information (SI). See DOI: https://doi.org/10.1039/d5ma01500f.

Acknowledgements

This work has been kindly supported by King Abdullah University of Science and Technology (KAUST).

Notes and references

1 D. W. Kweku, O. Bismark, A. Maxwell, D. A. Koomson, K. B. Danso, E. A. Oti-Mensah, A. T. Quachie and B. B. Adormaa, Greenhouse effect: Greenhouse gases and their impact on global warming, *J. Sci. Res. Rep.*, 2018, **17**(6), 1–9.
2 J. A. Patz, D. Campbell-Lendrum, T. Holloway and J. A. Foley, Impact of regional climate change on human health, *Nature*, 2005, **438**(7066), 310–317.
3 W. L. Filho, P. Perry, H. Heim, M. A. P. Dinis, H. Moda, E. Ebhuoma and A. Paço, An overview of the contribution of the textiles sector to climate change, *Front. Environ. Sci.*, 2022, **10**, 973102.
4 A. P. Raman, M. A. Anoma, L. Zhu, E. Rephaeli and S. Fan, Passive radiative cooling below ambient air temperature under direct sunlight, *Nature*, 2014, **515**(7528), 540–544.
5 F. L. Zhu and Q. Q. Feng, Recent advances in textile materials for personal radiative thermal management in indoor and outdoor environments, *Int. J. Therm. Sci.*, 2021, **165**, 106899.
6 K. Slater, Comfort properties of textiles, *Text. Prog.*, 1977, **9**(4), 1–70.
7 K. M. Faridul Hasan, S. Bai, S. Chen, K. Lin, T. Ahmed, J. Chen, A. Pan, Y. Zhu, C. S. Ki Lin and C. Y. Tso, Nanotechnology-empowered radiative cooling and warming textiles, *Cell Rep. Phys. Sci.*, 2024, 6.
8 A. P. Raman, M. A. Anoma, L. Zhu, E. Rephaeli and S. Fan, Passive radiative cooling below ambient air temperature under direct sunlight, *Nature*, 2014, **515**, 540–544.
9 J. Mandal, *et al.*, Hierarchically porous polymer coatings for highly efficient passive daytime radiative cooling, *Science*, 2018, **362**, 315–319.
10 Y. Zhai, *et al.*, Scalable-manufactured randomized glass-polymer hybrid metamaterial for daytime radiative cooling, *Science*, 2017, **355**, 1062–1066.
11 M. O. Faruk and M. M. Hossain, Smart and functional textiles for personal thermal comfort, *Smart Funct. Text.*, 2023, 329.
12 C. G. Granqvist and A. Hjortsberg, Radiative cooling to low temperatures: General considerations and application to selectively emitting sio films, *J. Appl. Phys.*, 1981, **52**(6), 4205–4220.
13 Y. Liu, H. Zhang, Y. Zhang, C. Liang and Q. An, Rendering passive radiative cooling capability to cotton textile by an alginate/caco3 coating *via* synergistic light manipulation and high water permeation, *Composites, Part B*, 2022, **240**, 109988.
14 S. Jiang, K. Zhang, C.-F. Wang, Q. Li, L. Zhu and S. Chen, Recent advancements in radiative cooling textiles for personal thermal management, *J. Mater. Chem. A*, 2024, **12**(25), 14866–14884.
15 L. Jiang, S. Zhou, J. Yang, H. Wang, H. Yu, H. Chen, Y. Zhao, X. Yuan, W. Chu and H. Li, Near-infrared light responsive tio2 for efficient solar energy utilization, *Adv. Funct. Mater.*, 2022, **32**(12), 2108977.
16 S. E. Keuleyan, *Mid-infrared mercury chalcogenide colloidal quantum dots*, The University of Chicago, 2013.
17 G. Gangisetty and R. Zevenhoven, A review of nanoparticle material coatings in passive radiative cooling systems including skylights, *Energies*, 2023, **16**(4), 1975.
18 M. Lee, G. Kim, Y. Jung, K. R. Pyun, J. Lee, B.-W. Kim and S. H. Ko, Photonic structures in radiative cooling, *Light: Sci. Appl.*, 2023, **12**(1), 134.
19 L. M. Degenstein, D. Sameoto, J. D. Hogan, A. Asad and P. I. Dolez, Smart textiles for visible and ir camouflage application: State-of-the-art and microfabrication path forward, *Micromachines*, 2021, **12**(7), 773.
20 X. Shan, L. Liu, Y. Wu, D. Yuan, J. Wang, C. Zhang and J. Wang, Aerogel-functionalized thermoplastic polyurethane

as waterproof, breathable freestanding films and coatings for passive daytime radiative cooling, *Adv. Sci.*, 2022, **9**(20), 2201190.

21 X. Li, Z. Ding, L. Kong, X. Fan, Y. Li, J. Zhao, L. Pan, D. S. Wiersma, L. Pattelli and H. Xu, Recent progress in organic-based radiative cooling materials: Fabrication methods and thermal management properties, *Mater. Adv.*, 2023, **4**(3), 804–822.

22 X. Wang, X. Liu, Z. Li, H. Zhang, Z. Yang, H. Zhou and T. Fan, Scalable flexible hybrid membranes with photonic structures for daytime radiative cooling, *Adv. Funct. Mater.*, 2020, **30**(5), 1907562.

23 A. Tolosana-Moranchel, C. Pecharromán, M. Faraldos and A. Bahamonde, Strong effect of light scattering by distribution of tio2 particle aggregates on photocatalytic efficiency in aqueous suspensions, *Chem. Eng. J.*, 2021, **403**, 126186.

24 J. Peoples, X. Li, Y. Lv, J. Qiu, Z. Huang and X. Ruan, A strategy of hierarchical particle sizes in nanoparticle composite for enhancing solar reflection, *Int. J. Heat Mass Transfer*, 2019, **131**, 487–494.

25 C. F. Bohren and D. R. Huffman, *Absorption and Scattering of Light by Small Particles*, John Wiley & Sons, 2008.

26 H. C. van de Hulst, *Light Scattering by Small Particles*, Courier Corporation, 1981.

27 P. K. Jain, K. S. Lee, I. H. El-Sayed and M. A. El-Sayed, Calculated absorption and scattering properties of gold nanoparticles of different size, shape, and composition: Applications in biological imaging and biomedicine, *J. Phys. Chem. B*, 2006, **110**(14), 7238–7248.

28 B. Zhu, W. Li, Q. Zhang, D. Li, X. Liu, Y. Wang, N. Xu, Z. Wu, J. Li and X. Li, *et al.*, Subambient daytime radiative cooling textile based on nanoprocessed silk, *Nat. Nanotechnol.*, 2021, **16**(12), 1342–1348.

29 V. Machado, A. Marinho, P. V. de Castro and T. Silva, From fabric to finish: The cytotoxic impact of textile chemicals on humans health, *Textiles*, 2025, **5**(2), 16.

30 G. Singh, J. Beddow, C. Mee, L. Maryniak, E. M. Joyce and T. J. Mason, Cytotoxicity study of textile fabrics impregnated with cuo nanoparticles in mammalian cells, *Int. J. Toxicol.*, 2017, **36**(6), 478–484.

31 H. Rabiei, M. Torshabi, M. Montazer, S. S. Khaloo and S. F. Dehghan, Antimicrobial activity and cytotoxicity of cotton-polyester fabric coated with a metal-organic framework and metal oxide nanoparticle, *Appl. Nanosci.*, 2023, **13**(8), 5765–5776.

32 X. Dong, Z. Wu, X. Li, L. Xiao, M. Yang, Y. Li, J. Duan and Z. Sun, The size-dependent cytotoxicity of amorphous silica nanoparticles: a systematic review of in vitro studies, *Int. J. Nanomed.*, 2020, 9089–9113.

33 J. Janovec, R. Agbaoye, J. Dolado and A. Ayuela, Size-dependent photonic and radiative properties of cao, sio2, al2o3 and fe2o3 cementitious oxides, *Sio2, Al2o3 and Fe2o3 Cementitious Oxides*.

34 Q. Wang, L. Deng, G. Zhou, Y. Zhu, R. Han and Y. Huang, High refractive index dielectric coating on plasmonic nanoantennas for strong visible light absorption in small transition metal nanoparticle reactors, *Opt. Lett.*, 2023, **48**(11), 3011–3014.

35 J. Song, J. Seo, J. Han, J. Lee and B. J. Lee, Ultrahigh emissivity of grating-patterned pdms film from 8 to 13 μm wavelength regime, *Appl. Phys. Lett.*, 2020, **117**(9), 1.

36 M. Batzill and U. Diebold, The surface and materials science of tin oxide, *Prog. Surf. Sci.*, 2005, **79**(2–4), 47–154.

37 S. Phromma, T. Wutikhun, P. Kasamechonchung, T. Eksangsri and C. Sapcharoenkun, Effect of calcination temperature on photocatalytic activity of synthesized tio2 nanoparticles *via* wet ball milling sol-gel method, *Appl. Sci.*, 2020, **10**(3), 993.

38 M. Pl Seah and W. A. Dench, Quantitative electron spectroscopy of surfaces: A standard data base for electron inelastic mean free paths in solids, *Surf. Interface Anal.*, 1979, **1**(1), 2–11.